scientific data

Check for updates

OPEN

DATA DESCRIPTOR

High-Density EEG and Multi-Muscle EMG Dataset during Object Prehension with a sensorized Grasping Box in Humans

G. Lomele[1], T. Lencioni[1], S. D'Ambrosio[1,2,3], A. Comanducci[1], F. Lucchetti[1], A. Marzegan[1], C. Derchi[1], S. Garzonio[2,4,5,6], T. Atzori[1], M. Rabuffetti[1], P. Castiglioni[1,7], M. Ferrarin[1,9] ✉ & L. Fornia[1,8,9]

Understanding how cortical areas control prehension movements requires synchronized neural and muscular data. For this aim, we introduce a novel open-access dataset of synchronized EEG and EMG recordings during prehension movements. The dataset combines high-density EEG (64 channels) with EMG recordings from 13 upper-limb muscles collected during prehension movements associated with 3 grip types: precision grip (thumb–index, PG), whole-hand power grasp (WH), and an unconventional grip (thumb–ring finger, UG). Data were acquired from 14 healthy participants performing visually guided prehension using a custom sensorized device that precisely timestamps action events, including go signals, object contacts, and lift completions. Each trial was divided into a dynamic phase (reaching, grasping, lifting) and a final isometric phase (holding), enabling investigation of transient and sustained motor activity. The extensive multi-muscle EMG recordings allow extraction of muscle synergy patterns that can be analyzed alongside EEG features to study cortico-muscular interactions. This dataset supports research on the neural control of complex hand movements, sensorimotor integration, and adaptive brain–computer interfaces. It provides a comprehensive resource for neuroscientists, engineers, and clinicians interested in motor control and its translation into rehabilitation practice.

Background & Summary

Understanding how the human brain orchestrates complex hand movements requires access to synchronized neural and muscular data. In recent years, open-access multimodal datasets combining electroencephalographic (EEG) and electromyographic (EMG) bipolar recordings have significantly advanced our ability to investigate the dynamic interplay between cortical and peripheral systems during voluntary motor behaviour[1,2]. Among the broad repertoire of human motor actions, visually guided object prehension stands out as one of the most ethologically significant behaviours, forming the basis for purposeful engagement with both the physical world and the social environment. Being one of the most sophisticated outcomes of primate sensorimotor evolution, grasping enables primates to manipulate objects, explore their surroundings, and respond adaptively to the demands of an ever-changing world. Numerous studies have demonstrated that this motor behaviour arises from the integrity of multiple large-scale cortico-subcortical and cortico-cortical pathways, which support sensorimotor integration and modulation of spinal circuits to generate context-appropriate motor output[3–8]. In parallel, this neural architecture has played a pivotal role in enabling tool use, gestural communication, and

[1]IRCCS Fondazione Don Carlo Gnocchi, Milan, Italy. [2]Department of Biomedical and Clinical Sciences, Università degli Studi di Milano, Milan, Italy. [3]Department of Clinical and Experimental Epilepsy, University College London, London, UK. [4]Department of Humanities and Life Sciences, Scuola Universitaria Superiore IUSS, Pavia, Italy. [5]Department of Neuroscience, Rehabilitation, Ophthalmology, Genetics, Maternal and Child Health, University of Genova, Genova, Italy. [6]Department of Rehabilitation, Azienda Socio Sanitaria Territoriale (ASST) Gaetano Pini - CTO, Milan, Italy. [7]Università degli Studi dell'Insubria, Varese, Italy. [8]Department of Medical Biotechnology and Translational Medicine, Università degli Studi di Milano, Milan, Italy. [9]These authors jointly supervised this work: M. Ferrarin, L. Fornia. ✉e-mail: mferrarin@DONGNOCCHI.IT

other survival-related functions throughout hominin evolution[9]. From a clinical standpoint, object prehension is frequently and sometimes persistently compromised in individuals with disorders affecting both central (e.g., stroke) and/or peripheral nervous system (e.g., neuromyopathy), highlighting its critical role in supporting autonomy and preserving a sustainable quality of life[10–12]. In this regard, gaining insight into how synchronized EEG and EMG signals reflect the mechanisms by which the central nervous system coordinates upper-limb muscle synergies during prehension may yield important discoveries in motor neuroscience.

Indeed, EEG provides a unique window into the temporal dynamics of cortical activity underlying motor planning and execution. Unlike neuroimaging-based techniques, EEG offers millisecond temporal resolution, making it ideally suited to capture the sensorimotor processing that controls hand-object interactions. When combined with EMG, it enables the characterization of bidirectional cortico-muscular interactions, including event-related desynchronization/synchronization (ERD/ERS) in sensorimotor rhythms, slow preparatory components such as the Bereitschaftspotential, and cortico-muscular coherence across different frequency bands. Furthermore, functional connectivity and cross-frequency coupling analyses can reveal how distributed cortical networks dynamically interact with peripheral effectors during grasp execution and maintenance.

From a translational perspective, such insights are instrumental for improving and designing next-generation brain–computer interfaces (BCIs) that are more adaptive, robust, and closely aligned with the principles of synergistic control[13–17].

To support the scientific community in addressing this challenge, we introduce here a novel open-access high-density EEG dataset synchronized with EMG recordings from 13 upper limb-hand muscles (including intrinsic and extrinsic hand muscles). The dataset was acquired in 14 healthy subjects during the execution of three distinct grasping actions: a precision grip (thumb–index opposition), a whole-hand power grasp, and an unconventional grip involving thumb–ring finger opposition. The choice of these specific grip types was motivated by both their functional significance in daily life and their potential to reveal distinct neural control strategies. Precision and power grips are the two most employed grasping patterns in daily life and have been widely investigated in neuroimaging studies, where they are known to engage partially distinct cortical and subcortical networks[18–21] and distinctive kinematic-muscular features[22–24]. Their inclusion in this study allows for the examination of well-characterized motor representations under simultaneous EEG–EMG conditions. In contrast, the third action, thumb-to-ring opposition, was selected as a rare and non-canonical grasp. This thumb-ring configuration, which is rarely employed in everyday motor behaviour, is particularly suitable for isolating the independent contributions of individual digits, making it an effective paradigm for studying fine finger control. As it is typically adopted only under specific biomechanical constraints, this action requires a level of digit individuation and thumb control unique to humans and absent in lower primates[25,26]. For instance, patients with ideomotor apraxia frequently exhibit a marked deficit in this non-canonical grip but not on the others[27]. All grasping actions were performed using a custom-built, sensorized grasping box designed to provide precise temporal labelling across successive motor events. Following the grip type instruction presented via a short movie followed by a two second resting phase, each trial began with a visual cue (*LED-on*, i.e. go signal) signalling reaching phase initiation, then a contact sensor detected the object *touch* event, and a limit-switch sensor indicated the completion of the pulling phase (*lift* event). The previous event marked the beginning of an isometric holding phase, which lasted until the LED was turned off (*LED-off* event was 5 seconds after *LED-on* event). After *LED-off* the hand left the grasp and returned to the starting point. This design allowed for the segmentation of each trial into two clearly defined temporal epochs of motor activity: a dynamic epoch encompassing reaching, grasping, and lifting, and a subsequent isometric holding phase during which the object was held steadily without further movement. This temporal structure provides a unique opportunity to dissociate the neural correlates of phasic versus isometric muscle activation.

Finally, the extensive multi-muscle EMG recordings allow for a reliable extraction of muscle synergies coefficients via decomposition methods that can be directly related to EEG-derived features. This dataset therefore provides a rich foundation for investigating how the brain encodes motor primitives during dynamic object interaction, as well as for exploring cortico-muscular coherence between cortical sources over sensorimotor areas and specific muscles during both phasic and isometric phases of the task.

In contrast to previously released EEG–EMG datasets, which have predominantly examined cyclic locomotion or planar reaching movements[28,29], the present dataset was specifically designed to capture the neural control of object-centred hand actions organized around ecologically meaningful motor sub-events. Existing resources typically lack: (i) reliable temporal segmentation of distinct motor sub-phases, (ii) the inclusion of both canonical and non-canonical grips enabling dissociation between habitual grasp patterns and uncommon digit configurations, and (iii) sufficiently dense EMG sampling across intrinsic and extrinsic hand muscles required to reconstruct muscle synergies. Consequently, the dataset enables not only the investigation of classical cortico-muscular coherence during isometric phase of the task[30], but also the characterization of coherence between cortical activity and synergy-level motor representations during phasic phases of action[31]. The present dataset specifically addresses this point by combining high-density EEG with extensive hand, forearm, and upper arm EMG recordings during visually guided object manipulation, while simultaneously providing precise event markers that dissociate movement initiation (reaching), object contact (actual grasping), lifting, sustained isometric holding and realising. Furthermore, several minutes of resting-state EEG were acquired for each participant, allowing the characterization of subject-specific spatial microstate organization and its relationship to subsequent motor behaviour[32].

Methods

Participants. 14 volunteer participants (13 right-handed and 1 left-handed, age: 31.4 + −10.4years, 7 males, 7 females) were recruited; participants did not present any pathology that affected the central or peripheral nervous system, the upper limb, spine or posture. This study was conducted following the principles of the Helsinki Declaration and was approved by the local Ethics Committee (Comitato Etico Territoriale Lombardia 4, protocol

number CET 73/24, 24 July 2024). Informed consent was signed by each participant before enrollment in any procedure, explicitly authorizing the collection of data, its scientific analysis, and its dissemination as an open-access dataset for research purposes.

Device and sensor setup, events and phases definitions. The experiments were conducted with a custom-built "grasping box" (Fig. 1A,B,F). The support platform was 3D-printed in plastic (L × W × H = 29,5 × 20 × 15,5 cm) and integrated, along one lateral edge, a coplanar extension set at a 45° incline to the horizontal. On this inclined surface, the grasp targets were mounted on a constant low-friction sliding carriage that allowed secure acquisition of the object and a controlled lifting motion of 2 cm executed along an oblique, ~45-degree direction. Each target comprised a larger square element (9,5 × 9,5 cm) with a smaller square insert (4,5 × 4,5 cm) positioned concentrically at its centre. This composite geometry enabled participants to perform all grip types required by the experimental protocol while preserving a constant setup, thus avoiding any interference with the standardized flow of the task.

A dedicated sensor suite and a software-controlled LED instrumented the device (Fig. 1B), allowing to identify go and stop events and between-events phases (touch, lift and holding). Two pressure sensors (Arcol Ohmite FSR07BE) were placed onto the upper surface of both small and big squares to detect first contact with the target to grasp and manipulate (*touch* event, Fig. 1B,C). These sensors were configured to operate as contact (on-off) triggers. This configuration was chosen to maximize temporal precision and minimize computational overhead on the data-acquisition unit, thereby ensuring a millisecond synchronization between behavioral events and electrophysiological recordings. At the distal end of the sliding bar, a contact (Microswitch ZF SPDT, 6 A, 250 V, IP50) monitored the end of the vertical displacement (*lift* event, Fig. 1G). The sliding bar was connected to a rubber band (elastic tensioner) to ensure uniform resistance to displacement across all participants and conditions. Finally, a LED (Knightbright, 2.5 V, 5 mm) mounted on the base immediately above the objects to be grasped, instructed the onset of the dynamic reaching-to-grasping phase (*LED–on* event) and the end (*LED–off* event) of the isometric holding phase. All sensor and LED channels were routed to a data-acquisition unit (Arduino UNO REV 3) that acquired triggers event time *(LED-on, touch, lift, LED-off* events*)* and transmitted them simultaneously to two separate computers, driving respectively EEG and EMG data acquisition, and enabling event-based temporal alignment across EEG and EMG (Fig. 1, bottom panel). Specifically, one computer handled EMG acquisition, stored triggers data, controlled *LED-on*/*LED-off* states, whereas the second computer managed EEG acquisition and recording of *LED-on* event and *LED-off* event data. In the released dataset, the events are provided as frame-pointers labeled *touch_event_frame, lift_event_frame, and LEDon_event_frame*, alongside the EEG and EMG analog traces.

EMG setup and acquisition. Wireless superficial bipolar EMG sensors (WavePlus, Cometa Systems Srl) were used. Specifically, 13 EMG sensors were positioned on the dominant upper limb. Muscles were selected to capture the hierarchical organization of grasping, spanning proximal arm stabilization, wrist orientation, global finger flexion–extension, and individuated digit control. Accordingly, we recorded anterior deltoid (DA), biceps brachii (BB), and triceps brachii (TB) to monitor proximal positioning and load support; extensor carpi radialis (ECR), extensor carpi ulnaris (ECU), flexor carpi radialis (FCR), and flexor carpi ulnaris (FCU) to characterize wrist stabilization; extensor digitorum communis (EDC) and flexor digitorum superficialis (FDS) to capture global finger configuration; and flexor pollicis longus (FPL), abductor pollicis brevis (ABP), first dorsal interosseous (FDI), and abductor digiti minimi (ADM) to quantify individuated digit control. Surface EMG electrodes were positioned reflecting a methodological trade-off between standardized landmarks[33] and the specific muscles required to probe the hierarchical organization of grasping (Fig. 2A). Electrode locations were adapted when necessary to accommodate the simultaneous recording of multiple adjacent muscles within the confined anatomical space of the forearm and hand, while minimizing crosstalk and possible mechanical interference between sensors. EMG data were recorded at 2 kHz using Cometa API integrated in our customized control software.

EEG setup and acquisition. EEG signals were recorded using a 64-channel amplifier (BrainAmp DC, Brain Products, Germany) from 62 scalp electrodes positioned according to the international 10/20 system (Fig. 2B). Electrode impedances were maintained below 5 kΩ, and data were sampled at 1 kHz. The reference and ground electrodes were both placed on the forehead. To monitor blink-eye movements, oblique bipolar EOG was recorded from two additional electrodes positioned at the outer canthi of the left and right eyes. This configuration increases sensitivity to both vertical and horizontal components of eye motion, thereby improving artifact detection and correction during subsequent preprocessing (e.g., ICA-based cleaning). Hardware filters were set at 10 s (≈0.016 Hz) and 250 Hz.

Experimental protocol. Each recording session began with the placement of the EEG cap and careful preparation of all electrodes (skin abrasion and conductive gel application) to ensure low impedance and optimal signal quality. Then EMG sensors were positioned on the arm. The patient was seated in front of the grasping box, with the non-dominant hand resting on the table next to the device support. The dominant hand was positioned in front of the device, with the elbow flexed at approximately 45° and the hand in a semi-closed posture (Fig. 1D)

The protocol started with a minimum of 5 minutes of resting with eyes open staring at a black screen, here only EEG is recorded. During the task, subjects were instructed to fixate on a screen. A fixation cross was first presented and lasted 2 seconds, followed by a video of 5 seconds illustrating the movement and in particular the type of grip to be executed. Immediately after the video ends, an on-screen arrow instructs the subject to fixate the LED positioned beneath the display, adjacent to the grasp targets. The fixation period lasted 2 seconds. This LED served as the go signal. At *LED-on* event, subjects performed the task, which consisted of four phases: 1) reaching towards the object, 2) actual grasping, 3) lifting and pulling until maximum displacement of the sliding

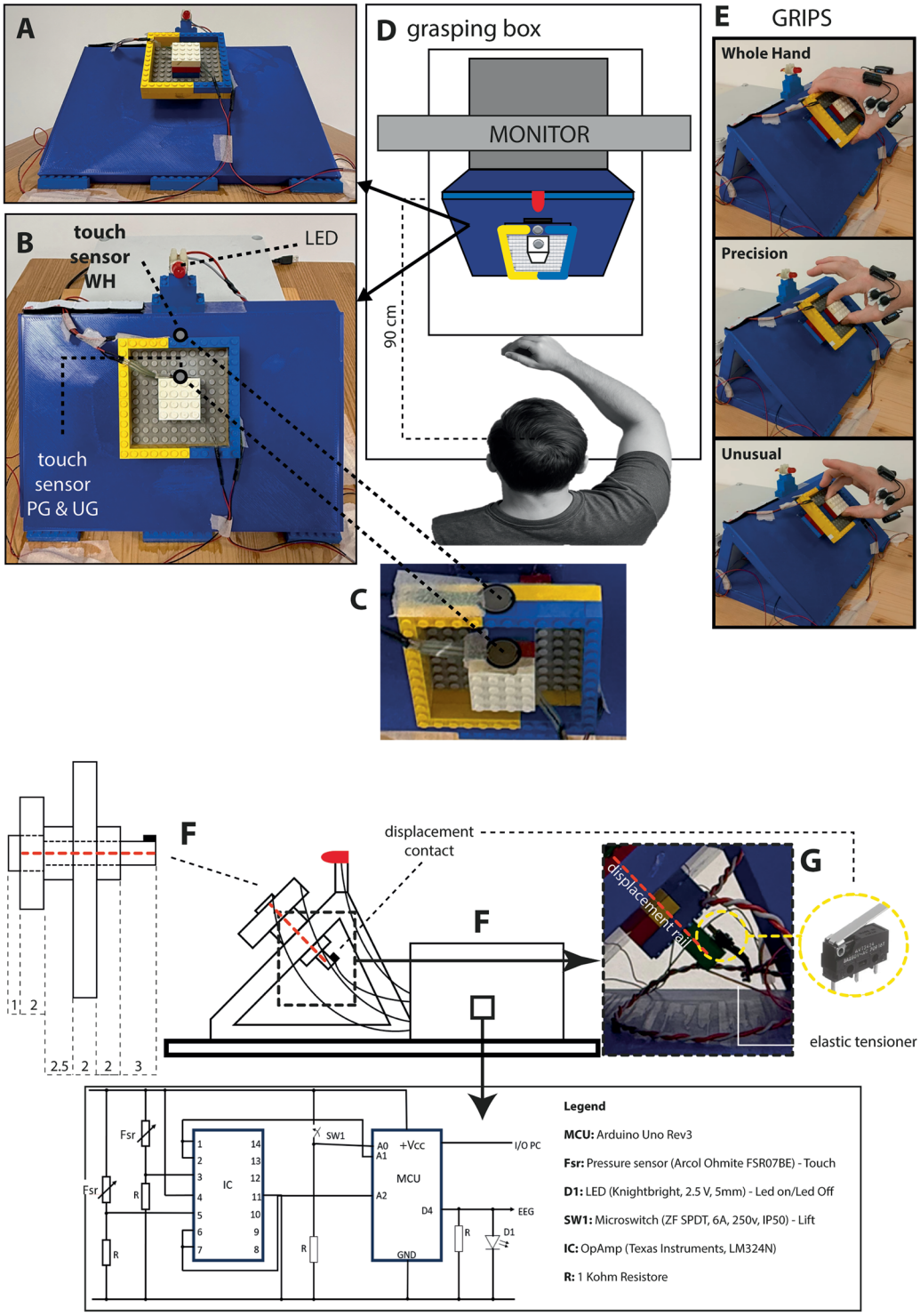

Fig. 1 Experimental setup, task components, and electronics. (**A**) **Front view** of the custom 3D-printed "grasping box" with the target mounted on a 45° inclined surface. (**B**) **Top-down view** highlighting the sensor locations: two pressure sensors (Fsr) are positioned on the large and small squares to detect the *touch* event for different grip types (WH vs PG/UG), and a central LED provides visual cues for the *LED-on* event (go signal) and *LED-off event* (end of hold). (**C**) **Close-up** of the concentric target geometry, designed to accommodate varying grasp sizes within a standardized setup. (**D**) Schematic of the participant's positioning relative to the device and the visual feedback monitor. (**E**) **Representative photographs of the three experimental grip types**: WH, PG and UG. (**F**) **Side-view** technical drawing illustrating the 45° oblique displacement rail and the position of the sliding carriage. (**G**) **Detail of the displacement mechanism**, showing the rail, the microswitch used to detect the *lift* event, and the rubber band used to provide constant mechanical resistance. Bottom panel. **Simplified electronic schematic of the data-acquisition unit**. An Arduino Uno (MCU) interfaces with the pressure sensors (Fsr) via an operational amplifier (IC) to generate digital triggers. These signals, along with the *lift* event (SW1) and LED (D1) status, are transmitted to the recording PCs to ensure synchronization between behavioral events and electrophysiological data (EEG/EMG).

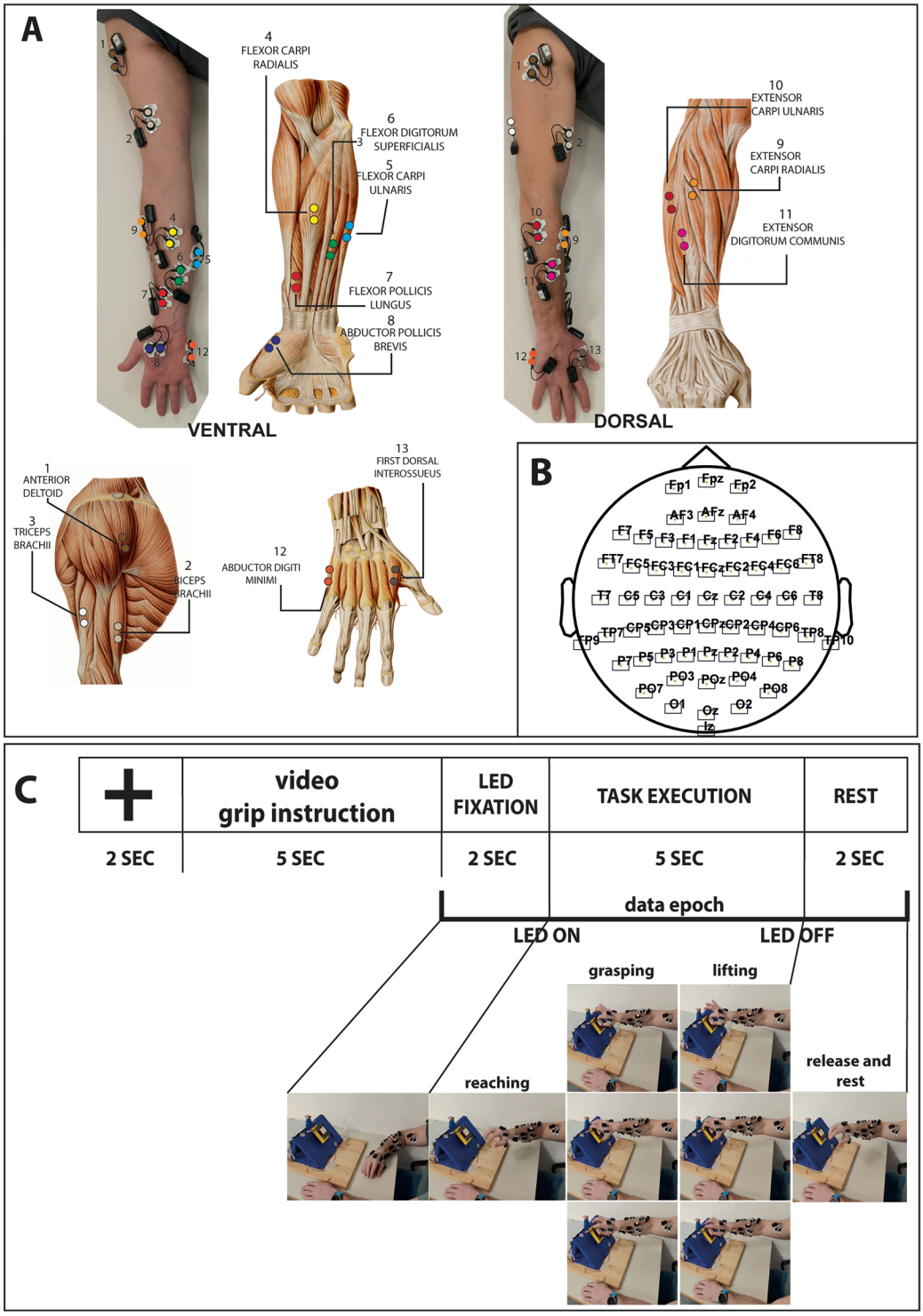

Fig. 2 Experimental paradigm and EMG electrode configuration. (**A**) **EMG sensor placement**. Distribution of the 13 wireless bipolar EMG sensors on the dominant upper limb. The configuration covers proximal muscles for stabilization (Deltoid, Biceps, Triceps), forearm muscles for wrist and finger control (Flexors and Extensors), and intrinsic hand muscles for individuated digit control (FPL, APB, FDI, ADM). Anatomical diagrams (ventral and dorsal views) illustrate the specific muscle targets according to the hierarchical organization of the grasping task. (**B**) **EEG electrodes placement**. Electrode layout of the EEG cap employed in the study, following the international 10–20 system. (**C**) **Experimental trial timeline**. Each trial follows a structured sequence: a fixation cross (2 s), followed by a video showing the grip instruction (5 s). After the video, a LED fixation period (2 s) precedes the "go" signal (*LED-on* event). The task execution phase (5 s) is time-locked to the LED and is divided into reaching, grasping, and lifting–holding phases. A final rest period (2 s) follows the *LED-off* event. The "data epoch" used for analysis extends from -2 s before *LED-on* to + 2 s after *LED-off* (total 9 s).

ID	SEX	AGE	Dominant Hand	Minutes of rest	Number of blocks	Total number of trials	Number of event-complete trials
1	M	31	RIGHT	5	5	148	148
2	F	25	RIGHT	0	4	120	104
3	M	28	RIGHT	10	4	120	100
4	F	43	RIGHT	10	3	90	88
5	F	21	RIGHT	10	3	90	80
6	F	21	RIGHT	10	3	90	83
7	F	59	RIGHT	6	3	90	45
8	F	23	RIGHT	6	4	120	110
9	M	27	RIGHT	5	4	120	109
10	M	33	RIGHT	10	4	120	120
11	M	35	RIGHT	11	4	120	115
12	F	28	RIGHT	10	4	120	120
13	M	25	RIGHT	10	4	120	120
14	M	41	LEFT	11	3	90	38

Table 1. Participant demographics and data availability. For each subject, the table reports ID, sex, dominant hand, age, minutes of rest recorded once before starting with the first block, number of executed blocks and the number of executed trials. Number of event-complete trials refers to trials containing all expected triggers, while the total number of trials includes all trials with at least the LED onset. Trials without valid pressure sensor activation or maximum sliding bar displacement reached were excluded from the event-complete number of trials.

bar in which the object is fixated and 4) holding in stable position the object until LED offset (LED-off). Then, subjects had to go back to the rest position and wait for the following fixation cross with a rest period of 2 seconds. Experimental paradigm is summarized in Fig. 2C.

Three grasp types were studied: precision grip (which require thumb–index opposition, PG), unconventional thumb–ring grip (UG), and whole-hand power grasp (WH), which require to grasp the bigger target using all the fingers (Fig. 1E). The manipulandum mounted on the grasping box imposed structural constraints that limited variability in finger placement. The spatial arrangement of the contact surfaces and embedded touch sensors required participants to interact with specific points on the object, thereby naturally constraining the position of the non-task digits and promoting a stable and reproducible hand configuration across subjects.

The experimental protocol comprised a minimum of three blocks, each containing at least 30 trials (10 per grip type), presented in fully randomized order. If a grip inconsistent with the video instruction was performed, the error was recorded and the trial was repeated at the end of the block. When participant conditions and available laboratory time permitted, additional blocks were recorded to increase the amount of available data. See Data Overview and Table 1 for details.

Data Record

Data pre-processing and data set preparation. EMG data were low-pass filtered using a 4th order Butterworth filter with cut-off frequency of 400 Hz and down-sampled at 1000 Hz to be comparable with EEG data. No pre-processing was applied to the EEG signals recorded both in resting state and during motor tasks. We segmented the EEG and EMG signals, in single trial data segments by pointing to the *LED-on* events on both EEG and EMG recordings: the EEG and EMG were segmented into trial-wise epochs time-locked to the *LED-on* event and lasting from −2 s relative to *LED-on* event to +7 s relative to *LED-on* event (total 9 seconds: from 2 s before *LED-on* event to 2 s after *LED-off* event), thereby capturing the full behaviour: from preparatory activity through reach–grasp–lift and the isometric hold and final release (Fig. 2C). The single trial data segments of both EEG and EMG were therefore natively synchronized by keeping the *LED-on* event, available on both recordings, as the pivot time point.

The dataset is available at the Open Science Framework (OSF) repository[34].

The repository contains electrophysiological recordings (EEG and EMG) acquired from 14 participants during a resting condition and during the execution of grasping tasks. Data are provided as MATLAB (.mat) files, with one file per participant.

For each participant (file named s_X.mat, where X denotes the participant number), a single MATLAB structure is provided. This structure contains a global struct (data) that is further divided into four sub-components: (i) subject-related information, (ii) general dataset metadata, (iii) baseline data (rest condition), and (iv) motor task data (trials). Across all participants (14 in total), the combined size of these data structures is 2.9 GB.

S_X.mat (14 files)

Each file contains all data referred to a single subject.

These files contain:

data.subject – Structure containing information about the participant.
.id – Subject id.
.age – Age of the subject.

.sex – Biological sex of the subject.
.hand – Dominant hand of the subject (LEFT or RIGHT).
data.info – Structure containing metadata about the recording.
.fs – Sampling frequency (Hz).
.eeg_channels – Structure with EEG channel information.
.labels – Channel name.
.X,.Y,.Z – Cartesian 3D coordinates of electrode positions (arbitrary units). X points to nasion, Y to left ear, Z upwards.
.sph_theta – Spherical horizontal angle (°) in XY plane, measured from nasion direction (positive = counter-clockwise).
.sph_phi – Spherical vertical angle (°), relative to XY plane (positive = upwards).
.sph_radius – Distance from origin (head center).
.theta – Polar angle (°) in 2D scalp projection, from nasion direction (counter-clockwise).
.radius – Normalized polar radius (0 = head center, 1 = scalp outline).
.emg_channels – List of 13 EMG channels.
.tasks_names – List of 3 tasks name.
data.baseline – Structure with signals during resting phase.
.eeg – EEG matrix (number of eeg channels × samples; channels names found in data.info.eeg_channels).
data.trials – Structure with signals recorded during each motor task trial. One entry per trial.
.eeg – EEG matrix (number of eeg channels × samples; channels names found in data.info.eeg_channels).
.emg – EMG matrix (number of emg channels × samples; channels names found in data.info.emg_channels).
.LEDon_event _frame– Index frame of *LED-on* event.
.touch_event_frame – Index frame of contact with pin (*touch* event).
.lift_event_frame – Index frame of maximum pin displacement (*lift* event).
.task – Index of performed task (names in data.info.tasks_names).
.block – Index of the recording block. Each block consisted of 30 trials (10 per grip type). While the standard protocol required three blocks (90 trials), additional blocks were acquired whenever participants were willing to continue and demonstrated sustained engagement with minimal signs of fatigue, thereby maximizing the amount of usable data collected.
.event_complete_trial – Boolean flag (1 = event-complete trial; 0 = incomplete trial). A value of 1 indicates that all critical task trigger events (*LED-on*, *touch*, and *lift*) were successfully captured. A value of 0 indicates that one or more triggers are missing, although the continuous EEG/EMG signals are still provided

Data Overview

Each participant completed a minimum of three blocks of 30 trials, comprising 10 trials per grip condition. Whenever laboratory time and the participant's condition allowed, additional blocks were acquired. The number of blocks completed, and the total number of trials acquired for each participant are reported in Table 1, together with participant demographics and overall data availability. In addition to ID, sex, age, dominant hand, and rest periods, the table reports both the total recorded trials and event-complete trials (trials where all events-trigger were successfully recorded). For instance, trials were classified as uncomplete if participants failed to activate the touch sensors and/or the lift–displacement sensor. Slight failures in trigger detection were not due to unsuccessful task execution; rather, minor variations in finger placement occasionally prevented direct contact with the sensor surface, resulting in missed triggers. Importantly, these trials still exhibited appropriate muscular activation patterns, indicating correct task performance. Trial with missing triggers are marked with event_complete_trial = 0 and retain full continuos EEG and EMG recordings, allowing future users to extract task-relevant epochs using alternative methods (e.g. EMG-based onset detection).

Technical validation analyses in this work were restricted to event-complete trials (.event_complete_trial = 1) and performed using subject-level normalization, ensuring that differences in the number of valid trials across participants do not bias group-level results. A detailed summary of the total number of trials and successfully recorded events is provided in Table 1.

Technical Validation

The dataset was validated with respect to temporal alignment between acquisition systems, signal integrity, and physiological plausibility of the recorded activity.

Synchronization between acquisition systems. The timing reliability of the concurrent EEG and EMG recordings, both nominally sampled at 1000 Hz, was evaluated by assessing the sampling frequency consistency between the two acquisition systems. Specifically, we quantified the difference in the number of samples detected by the EEG and EMG systems between two successive LED-on events, which occurred at a fixed interval of 16 seconds. At a nominal sampling rate of 1000 Hz, the expected number of samples within a 16-second interval is 16000. The mean difference between the two acquisition systems was 6.2 ± 0.7 samples across all subjects. This deviation corresponds to an estimated effective sampling frequency of approximately 1000.4 Hz for the EMG recording systems when assuming the EEG system sampled exactly at 1000 Hz. The resulting discrepancy (0.04% relative to the nominal sampling rate) is negligible and does not significantly affect typical analyses performed on the dataset. Furthermore, the difference remained constant across recording batches, indicating the absence

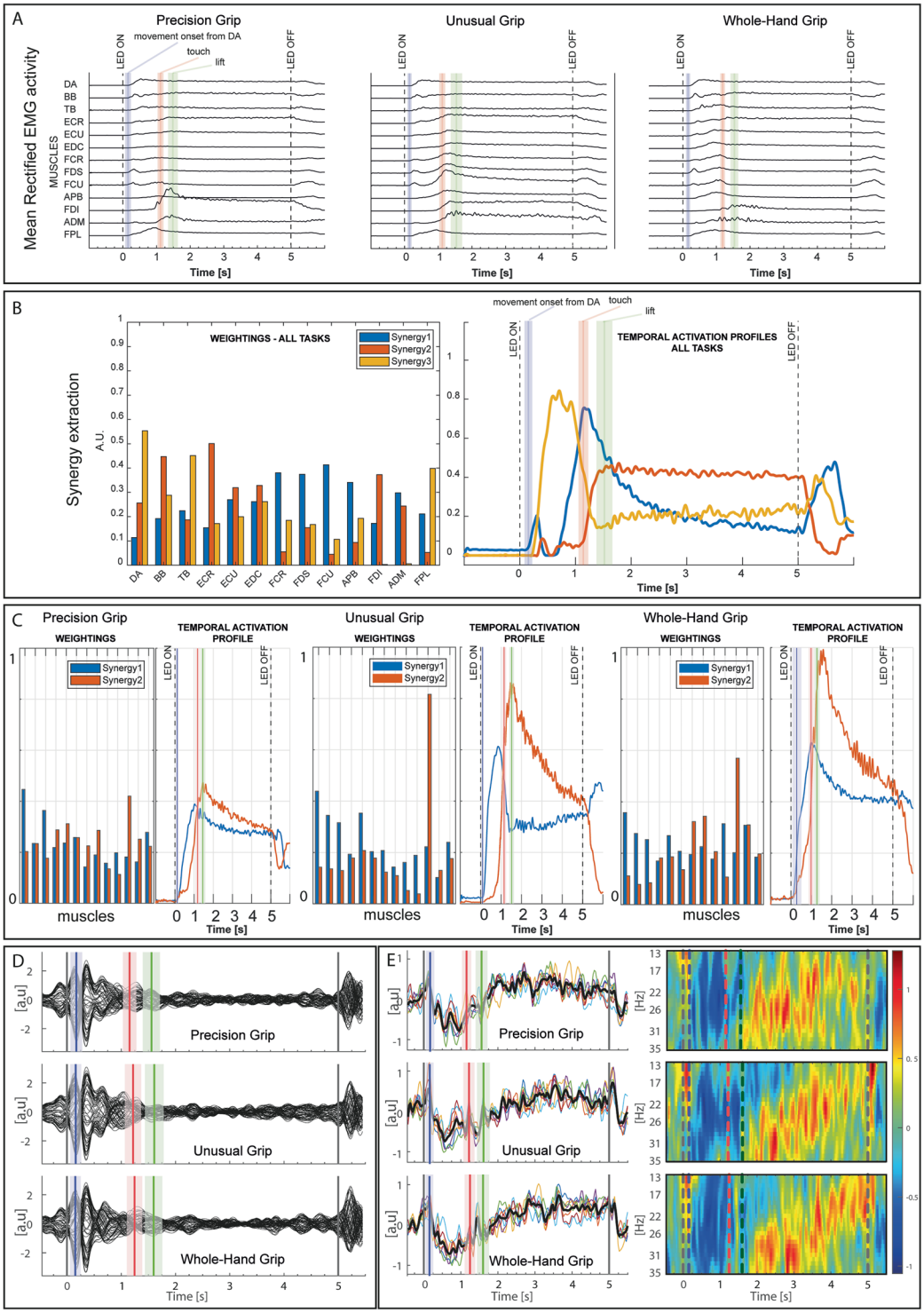

Fig. 3 Functional validation assessment. (**A**) **Example data from Subject 4: normalized EMG signal for the three tasks**. Normalized EMG signals for three grasping tasks (PG, UG, and WH). Bottom panels show the synergies extracted regardless of the performed grip (ALL TASKS). (**B**) **Example data from Subject 4: extracted synergies regardless of the task**. LEFT: Muscle weightings associated with each synergy. RIGHT: Temporal activation profiles for each synergy. Black vertical lines indicate *LED-on* event and *LED-off* event, and colored vertical lines with shaded areas represent key events with their standard deviation (*deltoid onset* event, *touch* event and *lift* event). (**C**) **Population level synergy extraction**. Data from subject 14 were excluded, as subject 14 was left-handed. Synergies identified in the three grasping tasks (PG, UG and WH) are common to at least 40% of the subjects. For each task, LEFT panel shows muscle weightings, averaged across subjects, associated with each synergy. RIGHT panel, represents activation profiles, averaged across subjects. Black vertical lines indicate *LED-on* event and *LED-off* event, and colored vertical lines with shaded areas represent key events with the standard deviation (deltoid onset, touch, lift). (**D**) **Population-level EEG movement-related cortical potentials**

(MRCPs). Data from subject 14 were excluded, as subject 14 was left-handed. Vertical lines indicate key task events (*LED-on* event, *deltoid onset* event, *touch* event, *lift* event, and *LED-off* event) along with their standard deviations. (**E**) **Population-level EEG beta-band activity**. Data from subject 14 were excluded, as subject 14 was left-handed. LEFT: percentage variation relative to baseline (–1 to –0.5 s before *LED-on* event) in motor-related channels (Cz, FCz, C3, C1, CPz, FC3, FC1). Vertical lines mark key events. RIGHT: Time–frequency representation of beta-band activity. percentage variation relative to baseline (–1 to –0.5 s before LED onset) in motor-related channels. Vertical dotted lines indicate task events (*LED-on* event, *deltoid onset* event, *touch* event, *lift* event, and *LED-off* event).

of progressive temporal drift between the systems. To ensure consistent temporal alignment across modalities, all task-related timestamps in the dataset are referenced to the LED-on signal, which was defined as time zero for each trial. This approach guarantees reliable synchronization across EEG, EMG, and behavioral signals while still allowing users to apply resampling procedures if desired.

Signal integrity and physiological plausibility. Signal quality was assessed by verifying the presence of well-established electrophysiological and muscular signatures associated with voluntary movement.

EMG data. EMG signals displayed consistent task-related modulation across the recorded muscles during the grasping task, reflecting coordinated muscle recruitment associated with object manipulation. Dimensionality-reduction approaches applied to the EMG activity further confirmed the presence of reproducible patterns of muscle co-activation across trials and participants, i.e. muscle synergies. More in details; for each participant, EMG signals from all recorded muscles were filtered, rectified, and converted into amplitude envelopes (Fig. 3A). Signals were then averaged across trials, both using pooled data and data separated according to the performed task. This procedure produced a data matrix describing the activity of all muscles over the execution time. To obtain robust estimates of muscle coordination patterns, synergy extraction was performed both using pooled data across all grasp types and by analyzing each grasp separately. The pooled representation was used only for visualization purposes (Fig. 3B). Muscle synergies were computed using non-negative matrix factorization (NMF) implemented in the Synergy Analyzer MATLAB toolbox[35]. This method decomposes the EMG dataset into two components: (i) a set of muscle weighting vectors describing the relative contribution of each muscle to each synergy, and (ii) time-varying activation profiles describing how strongly each synergy is recruited over time. The number of synergies was determined by progressively increasing the dimensionality of the decomposition and evaluating the reconstruction quality of the EMG signals. The smallest number of synergies explaining at least 92% of the variance of the original EMG signals was selected. To ensure stability, the factorization procedure was repeated multiple times with different random initializations, and the solution providing the best reconstruction of the EMG activity was retained. To assess consistency across participants performing the same task, the extracted synergy patterns were compared using cosine similarity. Synergies showing a similarity greater than 70% across subjects were considered to represent shared patterns (Fig. 3C).

EEG data. EEG data were band-pass filtered and visually inspected to identify noisy channels and artifacts. Channels exhibiting excessive noise were interpolated when necessary, and artifact-related components were removed using independent component analysis. EEG recordings exhibited clear movement-related cortical potentials (MRCPs) time-locked to the LED cue and task execution, as well as task-related modulation of sensorimotor beta-band activity (13–35 Hz) across sensorimotor channels. These features represent canonical neural markers of voluntary motor behaviour (Fig. 3D,E).

All validation procedures confirmed that the dataset contains temporally aligned multimodal recordings with physiologically plausible neural and muscular activity patterns, supporting its suitability for a broad range of analyses of human motor control.

Data availability

The data supporting the open source dataset are available at OSF (https://doi.org/10.17605/OSF.IO/RSV4Z)[34].

Code availability

The code supporting the open source dataset is available at OSF (https://doi.org/10.17605/OSF.IO/G6YTA)[36] (4.6GB). It contains pre-processed EEG and EMG and the code used to generate figures in *technical validation* section. Specifically, For EEG, both the fully raw recordings and ICA-cleaned datasets are provided. The ICA-processed EEG data are accompanied by all scripts and configuration files required to reproduce the complete preprocessing pipeline using the FieldTrip toolbox and to generate the figures presented in the manuscript. For EMG only the down-sampled signal is provided. EMG data are accompanied by all custom scripts and functions necessary to extract muscle synergies for each participant using the Synergy Analyzer toolbox. The code is organized into two distinct pipelines, as detailed in the accompanying README.txt file:

1. EEG Processing Pipeline – Requires MATLAB R2021a (or later) and the FieldTrip toolbox (https://www.fieldtriptoolbox.org/download/). All key analysis parameters (e.g., filter cutoffs, baseline intervals) are specified within the scripts. This pipeline reproduces the full preprocessing, group-level averaging, and plotting workflow for MRCPs and ERD/ERS analyses.

2. EMG & Muscle Synergy Analysis Pipeline – Requires MATLAB R2020a (or later) with the Signal Processing Toolbox. The Statistics and Optimization Toolboxes are recommended for the Non-negative Matrix Factorization

(NMF) implemented in SynergyAnalyzer.m. This pipeline includes all custom functions necessary for EMG pre-processing and muscle synergy extraction at single subject level.

Further details, including data structure, step-by-step instructions for running each pipeline, are provided in the README.txt file.

Received: 21 November 2025; Accepted: 13 April 2026;
Published online: 18 April 2026

References

1. Luciw, M. D., Jarocka, E. & Edin, B. B. Multi-channel EEG recordings during 3,936 grasp and lift trials with varying weight and friction, *Sci. Data*, **1**, https://doi.org/10.1038/sdata.2014.47 (2014).
2. Grosse, P., Cassidy, M. J. & Brown, P. EEG-EMG, MEG-EMG and EMG-EMG frequency analysis: physiological principles and clinical applications. [Online]. Available: www.elsevier.com/locate/clinph.
3. Errante, A., Ziccarelli, S., Mingolla, G. & Fogassi, L. Grasping and Manipulation: Neural Bases and Anatomical Circuitry in Humans, *Elsevier Ltd*. https://doi.org/10.1016/j.neuroscience.2021.01.028 (2021).
4. Turella, L. & Lingnau, A. Neural correlates of grasping, *Frontiers Media S. A*. https://doi.org/10.3389/fnhum.2014.00686 (2014).
5. Battaglia-Mayer, A. & Caminiti, R. Corticocortical systems underlying high-order motor control. *Journal of Neuroscience* **39**(23), 4404–4421, https://doi.org/10.1523/JNEUROSCI.2094-18.2019 (2019).
6. Lemon, R. N. Descending pathways in motor control. https://doi.org/10.1146/annurev.neuro.31.060407.125547 (2008).
7. Strick, P. L., Dum, R. P. & Rathelot, J.-A. *The Cortical Motor Areas and the Emergence of Motor Skills: A Neuroanatomical Perspective* **14**, 36, https://doi.org/10.1146/annurev-neuro-070918 (2025).
8. Bufacchi, R. J., Battaglia-Mayer, A., Iannetti, G. D. & Caminiti, R. Cortico-spinal modularity in the parieto-frontal system: A new perspective on action control, *Elsevier Ltd*. https://doi.org/10.1016/j.pneurobio.2023.102537 (2023).
9. Stout, D., Toth, N., Schick, K. & Chaminade, T. Neural correlates of Early Stone Age toolmaking: Technology, language and cognition in human evolution. *Philosophical Transactions of the Royal Society B: Biological Sciences* **363**(1499), 1939–1949, https://doi.org/10.1098/rstb.2008.0001 (2008).
10. Brandauer, B. *et al*. Impairments of prehension kinematics and grasping forces in patients with cerebellar degeneration and the relationship to cerebellar atrophy. *Clinical Neurophysiology* **119**(11), 2528–2537, https://doi.org/10.1016/j.clinph.2008.07.280 (2008).
11. Nowak, D. A. The impact of stroke on the performance of grasping: Usefulness of kinetic and kinematic motion analysis, https://doi.org/10.1016/j.neubiorev.2008.05.021 (2008).
12. García Álvarez, A., Roby-Brami, A., Robertson, J. & Roche, N. Functional classification of grasp strategies used by hemiplegic patients, *PLoS One*, **12**, 11, https://doi.org/10.1371/journal.pone.0187608 (2017).
13. Bizzi, E. & Cheung, V. C. K. The neural origin of muscle synergies. *Front. Comput. Neurosci.* **7**, 1–6, https://doi.org/10.3389/fncom.2013.00051 (2013).
14. Cheung, V. C. K. & Seki, K. Approaches to revealing the neural basis of muscle synergies: A review and a critique, *American Physiological Society*. https://doi.org/10.1152/jn.00625.2019 (2021).
15. Bizzi, E. & Ajemian, R. From motor planning to execution: a sensorimotor loop perspective. *J Neurophysiol* **124**, 1815–1823, https://doi.org/10.1152/jn.00715.2019.-How (2020).
16. Lanzarini, F. *et al*. Neuroethology of natural actions in freely moving monkeys. *Science (1979)*. **387**(6730), 214–220, https://doi.org/10.1126/science.adq6510 (2025).
17. Daly, J. J. & Wolpaw, J. R. Brain-computer interfaces in neurological rehabilitation. www.thelancet.com/neurology, **7** (2008).
18. Castiello, U. The neuroscience of grasping. *Nat. Rev. Neurosci.* **6**(9), 726–736, https://doi.org/10.1038/nrn1744 (2005).
19. Davare, M., Andres, M., Cosnard, G., Thonnard, J.-L. & Olivier, E. Dissociating the Role of Ventral and Dorsal Premotor Cortex in Precision Grasping. *The Journal of Neuroscience* **26**(8), 2260–2268, https://doi.org/10.1523/JNEUROSCI.3386-05.2006 (2006).
20. Begliomini, C., Wall, M. B., Smith, A. T. & Castiello, U. Differential cortical activity for precision and whole-hand visually guided grasping in humans. *European Journal of Neuroscience* **25**(4), 1245–1252, https://doi.org/10.1111/j.1460-9568.2007.05365.x (2007).
21. Ehrsson, H. H. *et al*. Cortical Activity in Precision- Versus Power-Grip Tasks: An fMRI Study. *J. Neurophysiol.* **83**(1), 528–536, https://doi.org/10.1152/jn.2000.83.1.528 (2000).
22. Santello, M., Flanders, M. & Soechting, J. F. Postural Hand Synergies for Tool Use. *The Journal of Neuroscience* **18**(23), 10105–10115, https://doi.org/10.1523/JNEUROSCI.18-23-10105.1998 (1998).
23. Thakur, P. H., Bastian, A. J. & Hsiao, S. S. Multidigit Movement Synergies of the Human Hand in an Unconstrained Haptic Exploration Task. *The Journal of Neuroscience* **28**(6), 1271–1281, https://doi.org/10.1523/JNEUROSCI.4512-07.2008 (2008).
24. Lapresa, M. *et al*. A comprehensive analysis of task-specific hand kinematic, muscle and force synergies. *Biocybern. Biomed. Eng.* **44**(1), 218–230, https://doi.org/10.1016/j.bbe.2024.01.006 (2024).
25. Häger-Ross, C. & Schieber, M. H. Quantifying the Independence of Human Finger Movements: Comparisons of Digits, Hands, and Movement Frequencies. *The Journal of Neuroscience* **20**(22), 8542–8550, https://doi.org/10.1523/JNEUROSCI.20-22-08542.2000 (2000).
26. Xu, J., Mawase, F. & Schieber, M. H. Evolution, biomechanics, and neurobiology converge to explain selective finger motor control. *Physiol. Rev.* **104**(3), 983–1020, https://doi.org/10.1152/physrev.00030.2023 (2024).
27. Fornia, L. *et al*. The parietal architecture binding cognition to sensorimotor integration: a multimodal causal study. *Brain* **147**(1), 297–310, https://doi.org/10.1093/brain/awad316 (2024).
28. Wagner, J. *et al*. High-density EEG mobile brain/body imaging data recorded during a challenging auditory gait pacing task. *Sci. Data* **6**(1), 211, https://doi.org/10.1038/s41597-019-0223-2 (2019).
29. Garro, F. *et al*. An EEG-EMG dataset from a standardized reaching task for biomarker research in upper limb assessment. *Sci. Data* **12**(1), 831, https://doi.org/10.1038/s41597-025-05042-4 (2025).
30. Luciw, M. D., Jarocka, E. & Edin, B. B. Multi-channel EEG recordings during 3,936 grasp and lift trials with varying weight and friction. *Sci. Data* **1**(1), 140047, https://doi.org/10.1038/sdata.2014.47 (2014).
31. Zandvoort, C. S., van Dieën, J. H., Dominici, N. & Daffertshofer, A. The human sensorimotor cortex fosters muscle synergies through cortico-synergy coherence. *Neuroimage* **199**, 30–37, https://doi.org/10.1016/j.neuroimage.2019.05.041 (2019).
32. Pirondini, E. *et al*. EEG topographies provide subject-specific correlates of motor control. *Sci. Rep.* **7**(1), 13229, https://doi.org/10.1038/s41598-017-13482-1 (2017).
33. Hermens, H. J., Freriks, B., Disselhorst-Klug, C. & Rau, G. Development of recommendations for SEMG sensors and sensor placement procedures, *Journal of Electromyography and Kinesiology* **10**(5) 361–374, https://doi.org/10.1016/S1050-6411(00)00027-4 (2000).
34. Lomele, G. *et al*. High-Density EEG and Multi-Muscle EMG Dataset during Object Prehension with a sensorized Grasping Box in Humans. [Online]. Available, https://doi.org/10.17605/OSF.IO/RSV4Z.
35. Russo, M., Scano, A., Brambilla, C. & d'Avella, A. SynergyAnalyzer: A Matlab toolbox implementing mixed-matrix factorization to identify kinematic-muscular synergies. *Comput. Methods Programs Biomed.* **251**, 108217, https://doi.org/10.1016/j.cmpb.2024.108217 (2024).
36. Lomele, G. *et al*. High-Density EEG and Multi-Muscle EMG Dataset during Object Prehension with a sensorized Grasping Box in Humans - scripts and preprocessed data. [Online]. Available, https://doi.org/10.17605/OSF.IO/G6YTA.

Acknowledgements
This work was supported by #NEXTGENERATIONEU (NGEU) and funded by the Ministry of University and Research (MUR), National Recovery and Resilience Plan (NRRP), project MNESYS (PE0000006)—A multiscale integrated approach to the study of the nervous system in health and disease (DN. 1553 11.10.2022). M.F and T.L were also supported by the European Union – NextGenerationEU (PNNR M4C2 – Investimento 1.5 Dalla ricerca all'impresa), under Grant ECS_00000035 (project "RAISE-Robotics and AI for Socio-economic Empowerment"). This work was also supported by the Ministry of Health under "Ricerca Corrente 2025–2027 program". S.D. was supported by ERC-2022-SYG Grant number 101071900 Neurological Mechanisms of Injury and Sleep-Like Cellular Dynamics (NEMESIS) and the Italian Ministry of Health—RicercaCorrente 2024.

Author contributions
Conceptualization, L.F. and M.F.; methodology, G.L., T.L., A.C., M.R., P.C., M.F. and L.F.; software, G.L., F.L., A.M., T.L. and M.R., validation, G.L., S.D., M.R. and L.F.; formal analysis, A.C., P.C., M.F. and L.F.; investigation, G.L., S.D., A.M., C.D., S.G. and T.A.; resources, M.F.; data curation, G.L., S.D. and L.F.; writing—original draft preparation, G.L. and L.F.; writing—review and editing, all authors; supervision, A.C., M.F. and L.F.; project administration and funding acquisition, M.F.

Competing interests
The authors declare no competing interests.

Additional information
Correspondence and requests for materials should be addressed to M.F.

Reprints and permissions information is available at www.nature.com/reprints.

Publisher's note Springer Nature remains neutral with regard to jurisdictional claims in published maps and institutional affiliations.